Chapter 15
Silicon-Based Anodes for Li-Ion Batteries

Ji-Guang Zhang, Wei Wang, Jie Xiao, Wu Xu, Gordon L. Graff, Gary Yang, Daiwon Choi, Deyu Wang, Xiaolin Li, and Jun Liu

Glossary

Li-ion battery	A family of rechargeable batteries in which lithium ions move from the negative electrode to the positive electrode during discharge, and back to the anode when charging.
Electric vehicle	Vehicle propelled by an electric motor (or motors) powered by rechargeable battery packs.
PHEV	Plug-in hybrid electrical vehicle. This is a hybrid vehicle with rechargeable batteries that can be restored to full charge by connecting a plug to an external electric power source.
Nanowire	A nanowire is a nanostructure, with the diameter of the order of a nanometer and aspect ratio greater than 10:1.
CVD	Chemical vapor deposition.
HEMM	High-energy mechanical milling.
Coulombic efficiency	The efficiency with which charge (electrons) is transferred in a system facilitating an electrochemical reaction.
Specific capacity	Capacity per unit weight of a battery (Ah/kg or mAh/g).
Specific energy	Energy per unit weight of a battery (Wh/kg).
Energy density	Energy per unit volume of a battery (Wh/l).

This chapter was originally published as part of the Encyclopedia of Sustainability Science and Technology edited by Robert A. Meyers. DOI:10.1007/978-1-4419-0851-3

J.-G. Zhang • W. Wang • J. Xiao • W. Xu • G.L. Graff (✉) • G. Yang • D. Choi • D. Wang • X. Li • J. Liu
Pacific Northwest National Laboratory,
Richland, WA, USA
e-mail: gl.graff@pnl.gov

R.J. Brodd (ed.), *Batteries for Sustainability: Selected Entries from the Encyclopedia of Sustainability Science and Technology*, DOI 10.1007/978-1-4614-5791-6_15,

Definition of the Subject

Silicon is environmentally benign and ubiquitous. Because of its high specific capacity, it is considered one of the most promising candidates to replace the conventional graphite negative electrode used in today's Li-ion batteries. The theoretical specific capacity of silicon is 4,212 mAh/g ($Li_{22}Si_5$) [1], which is 10 times greater than the specific capacity of graphite (LiC_6, 372 mAh/g). However, the high specific capacity of silicon is associated with large volume changes (more than 300%) when alloyed with lithium. These extreme volume changes can cause severe cracking and disintegration of the electrode and lead to significant capacity loss. Significant scientific research has been conducted to circumvent the deterioration of silicon-based anode materials during cycling. Various strategies, such as reduction of particle size, generation of active/inactive composites, fabrication of silicon-based thin films, use of alternative binders, and the synthesis of one-dimensional silicon nanostructures, have been implemented by a number of research groups. Fundamental mechanistic research also has been performed to better understand the electrochemical lithiation and delithiation processes during cycling in terms of crystal structure, phase transitions, morphological changes, and reaction kinetics. Although efforts to date have not attained a commercially viable silicon anode, further development is expected to produce anodes with three to five times the capacity of graphite. In this entry, an overview of research on silicon-based anodes used for lithium-ion battery applications is presented. The overview covers electrochemical alloying of the silicon with lithium, mechanisms responsible for capacity fade, and methodologies adapted to overcome capacity degradation observed during cycling. The recent development of silicon nanowires and nanoparticles with significantly improved electrochemical performance also is discussed relative to the mechanistic understanding. Finally, future directions on the development of silicon-based anodes are considered.

Introduction

Energy-storage technologies, particularly lithium-ion batteries, have been a focal point for development of advanced, fuel-efficient vehicles, especially plug-in hybrid electric vehicles (PHEVs). Although significant progress has been made during the last 20 years in various battery systems, existing systems do not satisfy all of the energy-storage needs for PHEV applications. More improvements are required with respect to energy density, power density, cycle life, safety, and cost. Commercial lithium-ion batteries primarily use graphite-based anodes, which have a theoretical specific capacity of 372 mAh/g (LiC_6). Continuous efforts have been made to find alternative anode materials, such as elemental metals, to replace graphite-based anodes since the early 1960s [2], when Dey first reported that lithium could be electrochemically alloyed with a number of metals at room temperature. Many elements such as aluminum (Al), silicon (Si), tin (Sn), antimony

Table 15.1 Specific capacities and molar volume changes exhibited by different candidate elements during cycling [5]

Elements	C	Al	Si	Sn	Bi
Lithiated phase	LiC_6	Li_9Al_3	Li_{21} Si_5	Li_{17} Sn_4	Li_3Bi
Theoretical specific capacity (Ah/kg)	372	2235	4012	959	385
Theoretical volumetric capacity (Ah/l)	833	6035	9340	7000	3773
Molar volume change (%)	12	238	297	257	115

(Sb), bismuth (Bi), magnesium (Mg), and zinc (Zn) are known to react with lithium to form alloys (see Eq. 15.1) by undergoing partially reversible electrochemical reactions that result in high specific and volumetric capacities.

$$Li_xM \leftrightarrow xLi^+ + xe^- + M \tag{15.1}$$

Among possible alternative alloying elements, silicon is the most attractive and widely investigated [3, 4] because of its high gravimetric and volumetric capacities and abundance in the natural environment. Silicon in the fully lithiated form of $Li_{4.4}Si$ provides a theoretical specific capacity of 4,212 mAh/g which is 10 times more than the capacity of graphite. The specific capacities and volume changes of the different electrochemically active elements are shown in Table 15.1.

Although the silicon-based anode has great potential, the alloying and subsequent de-alloying reactions during lithium insertion and lithium de-insertion result in severe crystallographic volume changes (~300% for silicon as shown in Table 15.1) because of various phase transitions. The mechanical strain generated during these phase transformations leads to cracking and disintegration of the electrode that, in turn, leads to failure of the anode after only a few cycles from loss of electrical contact between particles and the current collector. More details on the electrochemical alloying/de-alloying processes between lithium and silicon and the related failure mechanisms are discussed below. To prevent confusion, the following conventions are used in this chapter: discharge of silicon means lithium is inserted into silicon (lithiation or alloying of lithium with silicon); charge of silicon means lithium is de-inserted from silicon (delithiation or de-alloying of silicon).

Electrochemical Alloys of Lithium with Silicon

Studies of electrochemical alloys of lithium and silicon began with elemental lithium electrodes in high-temperature lithium/metal-sulfide secondary batteries [1, 6–8]. Lithium-silicon alloys with different stoichiometry were reported during the electrochemical lithiation of silicon at elevated temperatures (~400–500°C). The formation of $Li_{12}Si_7$, $Li_{14}Si_6$, $Li_{13}Si_4$, and $Li_{22}Si_5$ alloys was identified at distinct voltage plateaus according to each two-phase region, which follows the equilibrium lithium-silicon phase diagram as shown in Fig. 15.1. However,

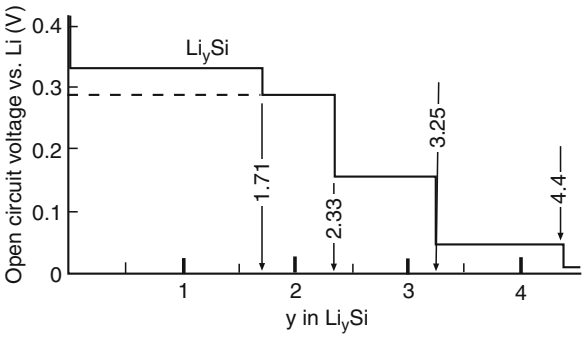

Fig. 15.1 Silicon lithiation showing two-phase plateaus at 415°C. (Reprinted with permission from Boukamp et al. [1]. Copyright 1981 The Electrochemical Society)

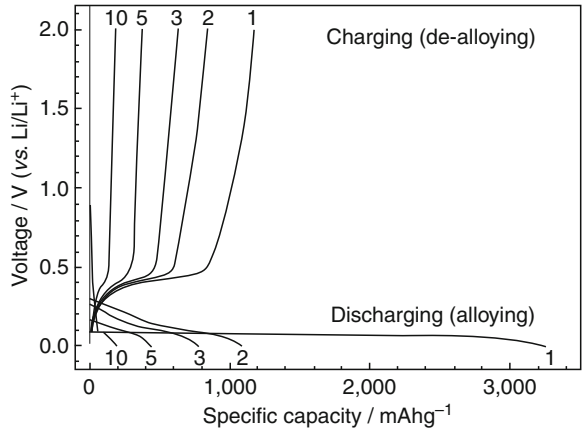

Fig. 15.2 Galvanostatic charge/discharge profiles for micro-silicon (10 μm) cycling at a current density of 100 mA/g in the voltage window of 0.0 –2.0 V (versus Li/Li^+) (Reprinted with permission from Ryu et al. [13]. Copyright 2004 The Electrochemical Society)

the electrochemical alloying process of lithium with silicon at room temperature was not readily understood because only one voltage plateau was observed for the silicon anode cycled between 0.0 V and ~1.2 V. Additionally, only ~3,500 mAh/g of capacity was obtained during the first discharge of a silicon anode at room temperature. Very few reports describing fundamental research on room-temperature electrochemical lithiation and delithiation of the silicon anode were published prior to the year 2000. Between 2000 and 2003, several groups observed that crystalline silicon undergoes electrochemical solid-state amorphization upon reacting with lithium at room temperature to form a metastable, lithium-silicon-based, amorphous phase where crystallization of the equilibrium intermetallic phases is kinetically suppressed [9–12]. The thermodynamically favored, high-temperature intermetallics do not easily crystallize at room temperature because of the sluggish kinetics.

Figure 15.2 shows the typical cycling performance of a pure crystalline silicon anode [13]. This sample has a discharge capacity of ~3,260 mAh/g, and a charge capacity of 1,170 mAh/g, which gives an irreversible loss of ~64%. Such a large irreversible capacity loss in the first cycle is commonly observed for silicon-based anodes when discharged to near-zero potential. The coexistence of an amorphous

lithium-silicon phase with the unreacted crystalline silicon leads to a single voltage plateau that is long and flat. This finding is consistent with results reported by several researchers who observed similar single, long, flat plateaus at ~0.1 V during electrochemical lithiation of crystalline silicon [3, 7, 9]. Though contrary to the equilibrium lithium-silicon phase diagram that shows multiple lithium-silicon phases [10, 14, 15], both ex situ and in situ X-ray diffraction (XRD) studies revealed a decrease and disappearance of the crystalline silicon peaks during the first lithium insertion, while no peaks corresponding to the equilibrium lithium-silicon phases were detected [10, 14, 15]. High-resolution transmission electron microscopy (HR-TEM) results confirmed that the lithiated silicon is formed primarily as an amorphous phase [10]. A change in the slope of the cell potential profile has been observed toward the end of the first discharge if the silicon anode is lithiated at an extremely low rate (~C/100), indicating formation of a new lithium-silicon phase. Obrovac and Christensen first reported the formation of a new crystalline phase when the highly lithiated amorphous silicon was electrochemically driven to ~50 mV versus Li/Li^+. Using XRD analysis, this new phase was identified as $Li_{15}Si_4$ [15]. Dahn et al. also confirmed the formation of $Li_{15}Si_4$ in both crystalline and amorphous silicon thin-film anodes when discharged below ~50 mV using in situ XRD analysis [14, 16]. Therefore, rather than forming the equilibrium $Li_{22}Si_5$ phase, $Li_{15}Si_4$ is the terminal phase that is achieved when the silicon anode is discharged to near-zero potential at ambient temperature. This phase renders a theoretical capacity of 3,579 mAh/g, a value that is in good agreement with most published reports on the silicon anode. It is worth noting that the formation of the $Li_{15}Si_4$ phase is observed only when the silicon anode is discharged at an extremely low rate (C/100). When the electrode is cycled at a moderate current rate (~C/10), the change of slope toward the end of the discharge is not observed. This characteristic provides further evidence of kinetically suppressed crystallization of lithium-silicon phases at low temperatures [17, 18].

Upon charge, the $Li_{15}Si_4$ phase delithiates to form an amorphous Li_ySi phase. The coexistence of these phases leads to a narrow potential window between ~0.3 V and 0.4 V, as shown in Fig. 15.2, which corresponds to the potential range of the de-alloying reaction. The in situ XRD study of the charge process and the XRD results from the chemical delithiation of the $Li_{12}Si_7$ phase have confirmed that the lithiated silicon becomes amorphous after charging [14, 15]. During the first discharge/charge process of the silicon-based anode, it is important to note that the formation of the $Li_{15}Si_4$ phase occurs only when the potential is driven below ~50 mV. Control of the cycling voltage above this value will bypass the formation of the $Li_{15}Si_4$ phase, leading to a different potential profile. For example, Obrovac [15] showed that a cell discharged to 0 V showed a change of slope at the end of the first discharge and a two-phase region during charging, both of which can be attributed to the formation of $Li_{15}Si_4$ phase. These two features are not present in the voltage profile of the cell cycled above 50 mV.

Amorphous silicon demonstrates different features than those of crystalline silicon when subjected to lithiation at room temperature. Studies on an amorphous silicon thin-film anode prepared by magnetron sputtering and an amorphous silicon anode obtained through chemical delithiation of $Li_{12}Si_7$ phase show two distinctive,

slightly sloping plateaus during the first discharge. These plateaus correspond to the two peaks observed in the dQ/dV curves [12, 15, 16]. The first peak is observed at ~0.2 V, which is about 0.1 V higher than the starting potential of lithiation observed in crystalline silicon. The second sloping plateau appears at ~0.1 V. The formation of the $Li_{15}Si_4$ phase also was identified in the amorphous silicon anode at a voltage ~30 mV. However, Dahn et al. reported that the crystalline phase only forms when the amorphous silicon thin films have a thickness greater than 2 μm. During the first lithiation, the amorphous silicon thin film that was cycled at a very low rate of C/48 exhibited a flat plateau at ~0.4 V, which may correspond to the conversion of the crystalline $Li_{15}Si_4$ phase to the amorphous Li_xSi. In comparison, the amorphous silicon thin-film anode cycled at a higher rate generally produced two broad humps at 0.3 V and 0.5 V, respectively. The phase formation of amorphous silicon during the first discharge/charge is not entirely understood. It generally is believed that the different peaks measured on the dQ/dV curves are related to the transition between different amorphous Li_xSi phases [17]. Because of the solid-state amorphorization discussed above, the voltage profile of the crystalline silicon anode and amorphous silicon anode exhibit similar features after the first charge/discharge cycle. The potential window in which silicon anodes operate is low enough to be useful in high-energy-density Li-ion batteries; however, Fig. 15.2 also reveals a large irreversible loss and rapid capacity fade during the lithium alloying/de-alloying process with silicon. These two problems have been reported by many researchers and are discussed in more detail below.

Failure Mechanisms of Bulk Silicon Anodes

The main challenge with the bulk silicon anode is the poor cycling stability as shown in Fig. 15.2. The reversible capacity decreases to less than 500 mAh/g by the fifth cycle. Several observations can be made concerning the rapid capacity fade from the charge/discharge profile. First, the irreversible loss is observed in every cycle, in contrast to conventional graphite anodes, where the irreversible losses cease after the initial one to two cycles. Second, although capacity fade occurs with every charge (i.e., de-alloying) cycle, upon re-discharging (alloying), the capacity recovers to approximately the same value measured in the previous charge cycle. This observation suggests that the degradation of the silicon anode is much more severe in the de-alloying cycle than in the alloying cycle.

There is strong evidence that failure of the silicon anode is caused by massive volume variations during lithiation and delithiation of the lithium-silicon alloys because the intermetallics formed have greater molar volume than the parent pure silicon phase. For example, $Li_{22}Si_5$ has a ~300% volume expansion over pure silicon, which causes substantial internal stress during lithiation or alloying. The fully lithiated phase of $Li_{15}Si_4$ exhibits a capacity of 3,579 mAh/g and has a density of 1.179 g/cm^3 calculated from XRD data, which represents

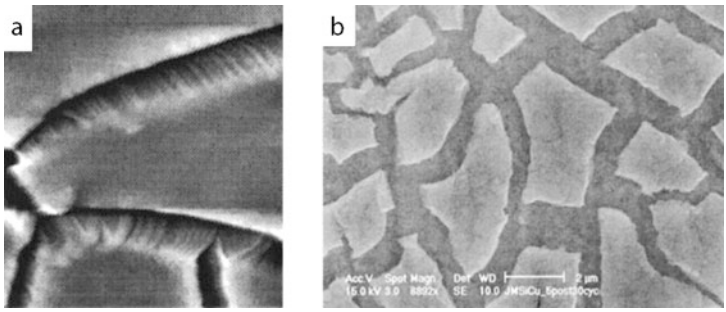

Fig. 15.3 (**a**) In situ AFM image showing the cracks of a silicon thin-film anode during cycling. (Reprinted with permission from Beaulieu et al. [20]. Copyright 2001 The Electrochemical Society) (**b**) SEM morphology of a 250-nm silicon thin film after 30 charges at a C/2.5 rate. (Reprinted with permission from Maranchi et al. [12]. Copyright 2003 The Electrochemical Society)

a volume expansion of 280% [19]. The amorphous Li_ySi alloy formed during discharging progressively undergoes volume expansion until formation of a final $Li_{15}Si_4$ intermetallic, which has nearly three times the volume per atom than the parent silicon. During the subsequent delithiation (de-alloying) process, the volume then contracts as lithium is extracted from the lithium-silicon intermetallic and amorphous phases [17, 20]. Crack formation and disintegration caused by the repetitive volume expansion and contraction are evident from the in situ atomic force microscopy (AFM) and scanning electron microscopy (SEM) images shown in Fig. 15.3 [12, 20]. The repeated volume expansion/contraction results in mechanical cracking and disintegration of the electrode, loss of electronic contact between active materials, and between active materials and current collector, thus rapid capacity fading.

A galvanostatic intermittent titration (GITT) study of the silicon anode shed more light on the poor cycling stability of the bulk silicon anode by measuring the variation in internal resistance during charge/discharge cycling [13]. In that study, a current of 100 mA/g was applied for 10 min, and then turned off for 20 min. A closed-circuit voltage (CCV) was measured while the current was on. A quasi-open-circuit voltage (QOCV) was obtained while the current was off. The internal resistance was then calculated from the difference between QOCV and CCV for each voltage transient. Figure 15.4 shows that, upon discharge, the internal resistance decreases, which is attributed to better electronic contact between the silicon particles resulting from the volume expansion during formation of Li_xSi alloys. One also could argue that the Li_xSi alloys have a slightly higher electronic conductivity than the pure silicon [19]. A drop in the internal resistance is observed below 0.3 V, which suggests that the alloying process primarily occurs below that voltage. During charge, the internal resistance increases because of increased contact resistance resulting from contraction of silicon particles/grains. Loss of electrical contact between particles leaves lithium ions trapped inside the anode (incomplete de-alloying) as the charge cycle is prematurely terminated when the electrode

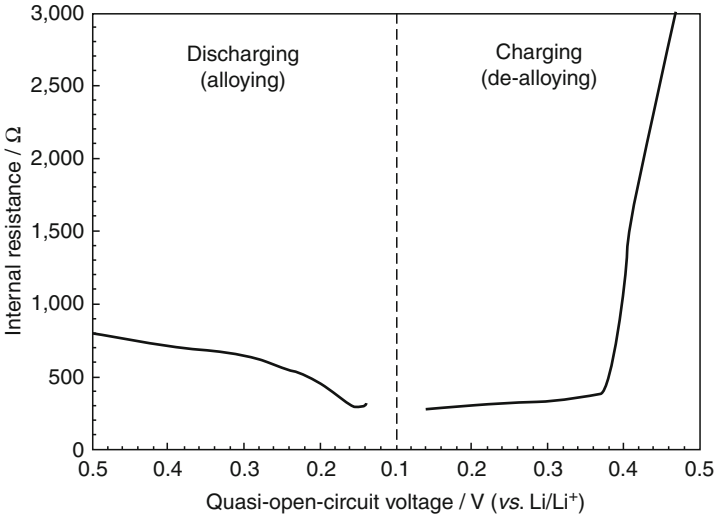

Fig. 15.4 Variation of internal resistance in a silicon anode (Reprinted with permission from Ryu et al. [13]. Copyright 2004 The Electrochemical Society)

potential exceeds the cycling potential window. Upon charge, an abrupt increase in internal resistance is seen above 0.4 V, which suggests that the de-alloying reaction occurs primarily above that voltage. These results confirm that failure of silicon anodes is caused by breakdown of the electronically conductive network resulting from the large volume changes and cracking of the native anode structures.

Strategies to Improve the Cycle Life of Silicon-Based Anodes

In recent years, tremendous research efforts have been made to improve the electrochemical performance of silicon-based materials. One strategy is to create a fine composite microstructure comprising an active lithium alloy phase uniformly dispersed in an inert host matrix, such as silicon/carbon, Si/TiB_2, or Si/TiN composite materials [22, 23]. Composites of silicon and carbonaceous materials have been reported to have enhanced cycle life. These can be made by chemical vapor deposition (CVD), pyrolysis of silicon-containing organic compounds, or by mechanochemical methods. The carbon increases the electrical conduction and also may accommodate the volume change of silicon and buffer the mechanical stress, thereby improving the cycle life. Another strategy is to develop various nanoscale silicon or silicon/carbon architectures, including one-dimensional nanowires, two-dimensional thin films, and three-dimensional composite architectures. This section will provide a brief review of various approaches used to improve the capacity and cycling stability of silicon-based anodes [24–26].

Active/Inactive Nanocomposites

Although nanostructured materials are known to exhibit superplastic behavior, it is difficult to envisage that even nanostructured silicon would survive mechanical degradation (cracking) after long-term cycling because of the large volume expansion/contraction. A concept that has been developed to capitalize on the attributes of nanostructured materials is the generation of electrochemically active/inactive composites [4, 27–29] in which the material reactive to lithium (termed as "active") is dispersed within materials that are nonreactive or less reactive to lithium (termed "inactive"). To generate a successful nanocomposite, both the active and inactive components need to be carefully selected to satisfy the requirement of low irreversible loss (20–30%), high capacity (>500 mAh/g), and good cyclability (~0.01% loss/cycle). Large volume changes are expected during the lithiation of silicon; therefore, the selection of matrix materials is of paramount importance to maintain the structural integrity.

The inactive components acting as the matrix usually consist of soft and ductile materials that play a very important role as "buffers" to alleviate the mechanical stresses arising from the large volumetric change of the active components. Increasing the inactive components in the electrode also was reported to suppress the aggregation of the active components upon cycling [30]. In this regard, inactive matrix components act as a skeleton or a network to form a microstructure that not only accommodates the volume changes, but also provides reaction sites for the active elements. Matrix materials also must exhibit good electronic and lithium-ion conductivity. Furthermore, the inactive matrix elements should be lightweight so that high gravimetric capacity can be achieved. Finally, the matrix materials should be inert to the active components because any reaction between matrix materials and active components will greatly reduce the useable capacity. The ratio between the active and inactive components is important to achieve the desirable cyclability and capacity. Previous reports show TiO_2 and ZrO_2 nanoparticles exhibit superplastic deformation [31], suggesting that other nanometer-size particles/phases may behave similarly and function as matrix components that accommodate structural changes upon cycling.

A schematic model of the "active/inactive" nanocomposite is shown in Fig. 15.5 [32]. Fuji Photo Film Celltec Company reported a tin-based amorphous composite oxide (TCO) [33] in 1997, which is the first demonstration of the "active/inactive" nanocomposite concept. In their results, the tin compound is the only active component reacting with lithium. The volume expansion of tin during cycling is reduced by the presence of other electrochemically inert oxide components including B_2O_3, P_2O_5, and Al_2O_3, which leads to good reversibility at a specific capacity of 800 mAh/g. The limitation of TCO is the large irreversible loss of >50% resulting from the electrochemical reaction depicted below.

$$SnO_2 + 8.4Li \rightarrow Li_{4.4}Sn + 2Li_2O \tag{15.2}$$

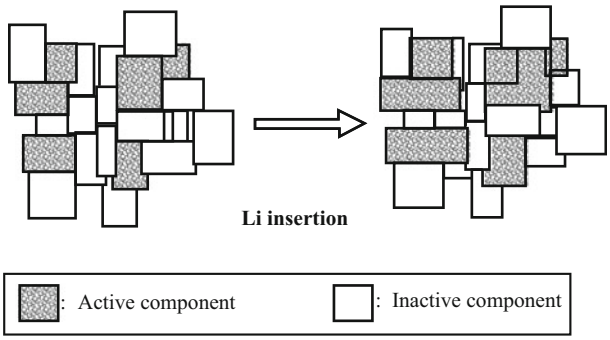

Fig. 15.5 Schematic model of the active/inactive nanocomposite and the morphological change occurring during lithium insertion Wang et al. [32]

The Li_2O formed in situ helps to bond the $Li_{4.4}Sn$ species but does cause a large irreversible loss of Li. Efforts have subsequently been made to synthesize composites containing the pure active phase (such as tin) in the electrochemically inactive phase, thus eliminating or minimizing the irreversible loss. Over the years, many different combinations of active and inactive systems have been investigated using two general approaches: (1) in situ nanocomposites and (2) ex situ nanocomposites. In the in situ approach, alloys or compounds such as Mg_2Si and SiAg are used as starting materials, and upon lithium insertion, the active phases (lithium-silicon alloys) are formed in situ with the less active phases or compounds [34, 35]. XRD and atomic emission spectroscopy (AES) studies showed that the lithium-silicon and lithium-magnesium alloys were formed during the first insertion [35]. The in situ approach relies on phase instability of the parent phases Mg_2Si and SiAg upon lithium insertion. Because magnesium and silver are high-density elements with large atomic masses, the net specific capacity that can be attained is only moderate. The availability of suitable compounds and the ability to synthesize such nanocomposites in the case of silicon also are very limited.

Like SnO_2, SiO was also investigated as a lithium-ion battery anode through the reduction of SiO in the first-discharge process to form, in situ, a silicon active phase and the compound Li_2O as the matrix, possibly according to the following reaction.

$$5SiO + 6Li \rightarrow 4Si + Li_2O + Li_4SiO_4 \tag{15.3}$$

Electrodes produced using this approach typically deliver a capacity of ~600 mAh/g with stable cycling, and could become an effective and low-cost route for preparing silicon-based anodes.

The ex situ approach relies on generation of active and inactive phases that are known to be thermodynamically stable. Thus, the lithium-ion reactions are confined to the active elements while the inactive phase(s) act as buffering agents to prevent electrode cracking/crumbling. The ex situ approach typically uses mechanical milling to form nanocomposites through mechanical alloying. The ex situ approach

is attractive because of the ease of sample preparation and the lack of chemical reactions between active and matrix components, even upon cycling. A number of systems studied as inactive materials have demonstrated limited improvements in the performance of the silicon anode [5]. Hard materials such as SiC have been used as the inactive material to curtail volume expansion during cycling. Kim et al. successfully achieved stable reversible capacities up to ~600 mAh/g by ex situ generation of amorphous silicon particles embedded within nanocrystalline matrices of SiC, TiN, TiB_2, and C [36–38].

Both inactive and active forms of carbon have been investigated as possible host matrices with finely divided silicon [36–38]. As with the inactive phases, active matrices must accommodate the volume changes in silicon and provide good mechanical strength and facile transport for both electrons and lithium ions. Of the various materials investigated in this approach, graphite is a good candidate as an active matrix material because of its good electronic conductivity and lubrication characteristics. In recent years, active/inactive and active/active silicon/carbon composites have attracted considerable interest and the electrochemical performance reported appears quite promising. The graphite matrix acts as a buffer to accommodate the large volume expansions of silicon while the silicon contributes to the overall capacity because of its large gravimetric and volumetric capacity. Various synthesis methods have been reported to prepare silicon/carbon composites and nanocomposites, ranging from high-energy mechanical milling (HEMM), pyrolysis, and physical mixing. The raw materials used include a variety of phases, such as crystalline and amorphous silicon, graphite, disordered carbon, mesoporous carbon, carbon nanotubes, and fullerenes. The following sections provide more detail on the various approaches used to produce silicon/carbon electrodes.

Silicon/Carbon Composites Prepared through Ball Milling

Mechanical milling can readily generate alloy systems with desirable compositions, structures, and particle sizes; therefore, HEMM has become a common approach for the synthesis of silicon/carbon composites. Results from different starting carbon materials such as graphite and disordered carbon [39] show a high first discharge and charge capacity (~800–1,400 mAh/g). However, the cycling stability is not as good as silicon/carbon composites derived from thermal pyrolysis of silicon-containing polymers. Gross et al. [40] reported a first-lithiation capacity of ~800 mAh/g with a fading rate of ~1.25% for a composite made by 15-min mechanical milling of graphite and a pre-milled silicon powder. The poor capacity retention is likely caused by the large silicon particles (>1 μm) in the composite. These particles disintegrate because of volume changes during lithium alloying and de-alloying processes, as discussed above. This hypothesis suggests that extended milling may improve the cycling stability by decreasing the silicon particle size and homogeneously distributing silicon particles in the graphite matrix. However, extended milling leads to formation of electrochemically inactive SiC because of

mechanochemical reactions between silicon and carbon [37]. In addition to the formation of SiC, amorphization of graphite during prolonged milling also prevents stable high-capacity cycling of the silicon/carbon composite. Several polymer additives have been identified that serve as effective diffusion barriers to circumvent the formation of SiC and preserve the graphite structure during prolonged milling. Kim et al. [41] reported nanocomposites of silicon/carbon with a capacity as high as ~850 mAh/g and reasonable capacity retention (~1.1% loss/cycle). These nanocomposites were synthesized from silicon and polystyrene (PA resin) using HEMM. Datta et al. [22] recently reported methods to stabilize a composite using silicon, graphite, and polyacrylonitrile-based disordered carbon through HEMM, followed by subsequent heat treatment.

Si/C Composites Prepared Through High-Temperature Pyrolysis and CVDProcesses

In addition to the selection of appropriate starting materials to form active/inactive or active/active composites, the synthesis method must be carefully chosen to generate materials with desired properties. Recently, several novel methods including CVD, physical vapor deposition (PVD), and templated growth have been developed to generate nanoscale and nanostructured silicon-based materials. Control of structure, particle size, and composition of silicon/carbon composites using CVD or pyrolysis reactions is difficult. In addition, maintaining a homogeneous distribution of silicon throughout the sample, which is a critical attribute for good cycling performance, is particularly challenging. In general, the chosen method should synthesize composites containing discrete phases without any chemical interaction to prevent loss of the active component and minimizing subsequent loss of electrochemical capacity.

Decomposition of organic precursors is one of the most common approaches investigated. Dahn et al. [42] systematically studied the pyrolysis of different silicon-containing polymers during the mid-1990s. More recent results include thermal pyrolysis of polyvinyl chloride dispersed with nanosized silicon and fine graphite particles to achieve a reversible capacity of ~700 mAh/g as reported by Yang et al. [43]. The same group also reported similar results from pyrolysis of pitch embedded with graphite and silicon powders [43]. However, silicon/carbon composites synthesized by pyrolysis of silicon-containing polymers suffer from a large irreversible loss (~50–60%) in the first cycle mainly because of the presence of disordered carbon and sulfur/oxygen/hydrogen impurities generated during high-temperature decomposition.

Another high-temperature approach for generating silicon/carbon composites is to deposit silicon particles on carbon or vice versa using CVD. Xie et al. [44] reported the deposition of silicon on mesocarbon microbeads (MCMB) by CVD of silane at 450°C and 500°C, but only a very small amount of silicon actually deposited on the MCMB. The material also demonstrated a very high (55%) irreversible loss. Vacuum deposition of nanometer-sized silicon particles on graphite surfaces has also been reported [45, 46]. The as-prepared anode showed an

irreversible capacity loss of 26% with a capacity fade rate of less than 1% over 100 cycles. This cycling performance probably is one of the best reported for a silicon/carbon composite, and is attributed to the nanoscale silicon particle size (~50 nm) and strong adhesion of the silicon particles with the graphite matrix. In an attempt to reduce irreversible loss, carbon also has been deposited on pure silicon powders [47, 48]. However, the electrochemical performance of these materials was inferior to the silicon/carbon composite generated by depositing silicon on the carbon surface.

Silicon/Carbon Nanotube Composites

Recently, carbon nanotubes (CNTs) also were investigated as candidate matrix materials. CNTs possess certain unparalleled characteristics that could be valuable in producing stable silicon/carbon composite anodes. The diameter of single-wall nanotubes (SWNTs) is in the range of 1–10 nm, while that of multiwall nanotubes (MWNTs) is in the range of ~100 nm. CNTs can be several microns in length, resulting in aspect ratios greater than ~1,000. Their specific surface area (SSA) is usually greater than 500 m^2/g. Strong C=C bonding to three adjacent neighboring atoms results in excellent mechanical properties in CNTs. The Young's modulus of SWNTs is approximately 1 TPa, and the maximum tensile strength is ~30 GPa [49]. Treacy et al. [50] reported an elastic modulus as high as 1.25 TPa. These values compare well with the modulus of MWNTs (1.28 TPa) measured by Wong et al. [51]. High tensile strengths up to ~63 GPa have been reported for MWNTs [52], which is an order of magnitude higher than that of carbon fibers and stainless steel (~5 GPa and ~3 GPa, respectively). The unique bonding structure also enables exceptional flexibility. The theoretical maximum elongation of an SWNT is almost 20% [53]. CNTs also are highly resistant to damage from external forces. Application of force to a nanotube typically results in bending, but not permanent damage. When the force is removed, the tube returns to its original state [54]. With respect to electrical conductivity, both MWNTs and SWNTs are excellent electrical conductors. The resistivity of SWNT ropes is approximately 10^{-4} Ω-cm at 300 K or roughly on the same order of magnitude as graphite [55]. MWNTs can carry extremely high current densities that exceed 107 Acm^{-2}, while a current density of 109 Acm^{-2} has been reported in SWNTs [56, 57]. These values clearly exceed the electrical property requirement of lithium-ion anodes. All of these attributes suggest that CNTs would be good candidates for matrix materials. The high-aspect-ratio, one-dimensional structures can form entangled three-dimensional networks that maintain electrical contact with silicon particles during cycling. The unusual flexibility and elongation could further facilitate stability, particularly after the active materials undergo cracking and disintegration. Finally, the high electrical conductivity and current density, combined with the low material density, could produce unprecedented matrix properties.

Although promising, in practice, the high irreversible loss and large voltage hysteresis during electrochemical cycling greatly limit the use of CNTs as active

anode materials in lithium-ion batteries. Shu et al. [58] reported the synthesis of CNT-based silicon/carbon composites by decomposition of acetylene at 800°C using a nickel-phosphorus catalyst deposited on the silicon particles to seed nanotube growth. This silicon/carbon composite anode demonstrated a first cycle discharge capacity of 1,120 mAh/g and an irreversible loss of 20%. Wang et al. [59] achieved a capacity of ~1,000 mAh/g by homogenously dispersing a pre-milled silicon/graphite powder into a single-wall carbon nanotube matrix using ultrasonication. Si et al. [60] reported that the direct mixing of carbon nanofibers with carbon-coated silicon nanoparticles helped to maintain a stable cycling for the silicon-based anode. When carbon nanofibers are used as the current collector, superior overall capacity, cyclability, and rate capability have been demonstrated [61]. Lee et al. [62] also reported the use of wet ball milling to thoroughly mix silicon starting materials with different carbon sources, including single-walled and multiwalled CNTs. Although a high first-discharge capacity of ~2,000 mAh/g was achieved, rapid capacity fade was observed after 15 cycles [62]. Generally, anodes generated from simple mixtures of silicon particles and CNTs show poor capacity retention, but significant improvements were observed when silicon was directly deposited, using silane-based CVD, onto the CNTs or carbon nanofibers. The performance improvements were attributed to the formation of strong bonding layers between the silicon cluster and the CNT surface, which helped facilitate transport of lithium ions and electrons, in addition to the relaxation of stresses generated from the repetitive volume changes [18, 63].

Nanoscale Architectures

Several research groups have reported that reduction of the particle size leads to better accommodation of the strain generated during lithium insertion/de-insertion, therefore resulting in improved cycling performance. Although this work initiated with tin-based anode materials, the same strategy soon was applied to silicon-based systems by Yang et al. [64–66]. Huggins et al. [67] also suggested that decrepitation leads to a critical particle size more tolerant to mechanical stress. Researchers have reported superior electrochemical performance of nanoscale, over bulk, silicon, and attributed the performance to better strain accommodation in the smaller particles [68].

Generation of nanosized particles (~1–100 nm) results in a relatively low number of atoms per grain, less volume change upon cycling, and therefore, reduced mechanical stresses within the particles. In addition, the large number of grain boundaries existing in nanosized materials may help stabilize the particles and also act as channels for lithium insertion and de-insertion [69]. Other advantages include increased contact area between particles, within the electrode, and between the electrode and electrolyte, all leading to higher charge/discharge rates. Nanosized systems also provide a shorter diffusion path for the transport of both

electrons and lithium ions, which improves performance for materials exhibiting poor electronic or lithium-ion conductivity. Another possible benefit of nanostructured materials is the potential to undergo superplastic deformation during cycling to better accommodate strain generated by large volumetric changes. Equation 15.4 describes the relationship between applied stress (σ), temperature (T), grain size (d), and the resulting strain rate ($\dot{\varepsilon}$) [31].

$$\dot{\varepsilon} = A\sigma^{n}d^{-p}D_0 \exp(-Q/RT) \tag{15.4}$$

where A is a constant, n is the stress exponent ($n \approx 2$), p is the grain size exponent ($p \approx 2$–3), Q is the activation energy, and R is the gas constant. An examination of Eq. 15.4 reveals that the strain rate for nanocrystalline materials will be several orders of magnitude higher than that of conventional-sized (i.e., micron-sized) materials at the same temperature. Therefore, nanostructured materials could possibly achieve appreciable superplastic strain at room temperature and are more suitable for use as anode materials. Nanocrystalline materials can be either single-phase or multiphase materials, which are in the size range of about 1 nm to 100 nm. Compared to materials containing larger grain sizes, the nanocrystalline materials generally exhibit improved mechanical hardness, fracture toughness, and ductility because of the large fraction of the atoms located at surfaces or grain boundaries [70]. Therefore, using nanocrystalline materials as anodes will enhance not only the diffusion rates because of higher grain-boundary diffusion, but also the overall mechanical strength of the anode. Recently, this nanoscale synthesis approach has expanded into the growth of one-dimensional silicon nanowires and silicon nanoparticles with demonstrated superior electrochemical cycling performance, as will be discussed in a later section.

Two-Dimensional Silicon Thin-Film Anodes

Inspired by the improved performance of nanoscale-sized silicon particles over bulk silicon particles, many groups have tested silicon thin films deposited on metallic substrates (e.g., copper or nickel), in which the thin-film silicon contains nanometer-sized silicon features. In general, thin-film silicon anodes can be classified into nanocrystalline thin-film anodes and amorphous thin-film anodes. Graetz et al. [71] prepared nanocrystalline silicon thin-film anodes using PVD. These anodes exhibited specific capacities of approximately 1,100 $mAhg^{-1}$ with a 50% capacity retention after 50 cycles. The improved electrochemical performance of the thin-film anode was linked to good adhesion between deposited silicon particles and the substrate current collector.

Because of isotropic expansion of the particles/grains, amorphous thin-film silicon anodes typically perform better than crystalline thin films. Maranchi et al. [12, 72] demonstrated that 250-nm-thick amorphous silicon thin films deposited by radio-frequency magnetron sputtering on copper substrates achieved near theoretical capacity for a limited number of cycles. The authors stated that growth of

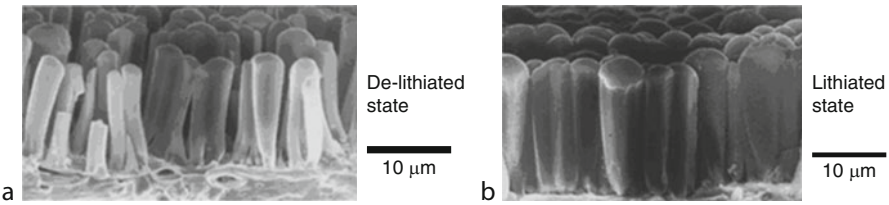

Fig. 15.6 Cross-sectional SEM images of an a-silicon thin-film electrode in the (**a**) de-lithiated and (**b**) lithiated states (Reprinted with permission from Yonezu et al. [77]. Copyright 2004 The Electrochemical Society)

a lithium-copper-silicon phase at the interface between silicon and copper, and the incremental plastic strain in the copper substrate upon cycling, resulted in a reduction of adhesion between the silicon film and the current collector, and progressive failure of the silicon film. Good electrochemical cycling performance also has been reported for multicomponent thin films, such as submicron-sized iron/silicon multilayer films and alternating cobalt/silicon layers [73, 74].

Surface roughness of the substrate can significantly influence the performance of silicon thin films [75, 76]. Yonezu et al. [77] reported that an amorphous silicon (a-silicon) film sputtered on a moderately roughened copper foil achieved virtually 100% reversibility with a corresponding capacity greater than 3,000 mAh/g. The as-deposited a-silicon film (5-μm thick) grew to a thickness of 17 μm during the first full charge. After the first cycle, the silicon thin film divided into micro-columns.

Figure 15.6a, b show that the micro-columns of lithium-silicon predominantly expand/contract along the column diameter. This preferential expansion may directly relate to minimization of surface tension and surface energy in the given structures. Although these sputtered a-silicon thin films show excellent capacity and cycle performance, materials prepared by sputtering are not economical for large-scale, high-volume applications. Another serious limitation is that the practical electrode thickness attainable using vacuum deposition is not useful for anodes in large-scale applications such as PHEVs. If silicon nanorods can be prepared, using scalable synthesis routes, and that retain the high aspect ratio (similar to those shown in Fig. 15.6), it is reasonable to expect that the lithium-silicon nanorod would expand/contract preferentially along its diameter and maintain mechanical integrity during lithium insertion/de-insertion. Anodes with capacities >600 mAh/g and improved mechanical/structural stability over silicon thin films or bulk powders would be possible. Such developments could enable the use of silicon nanorod anodes in large-scale applications such as PHEVs and other commercial applications.

Another approach involves dispersing silicon nanoparticles with graphene sheets to form another class of two-dimensional, silicon-based nanostructures in which the silicon particles are in intimate contact with the graphene. In this method, regions of graphene restack to form a graphite network that anchors the more flexible graphene and provides a highly electronically conductive matrix. The highly

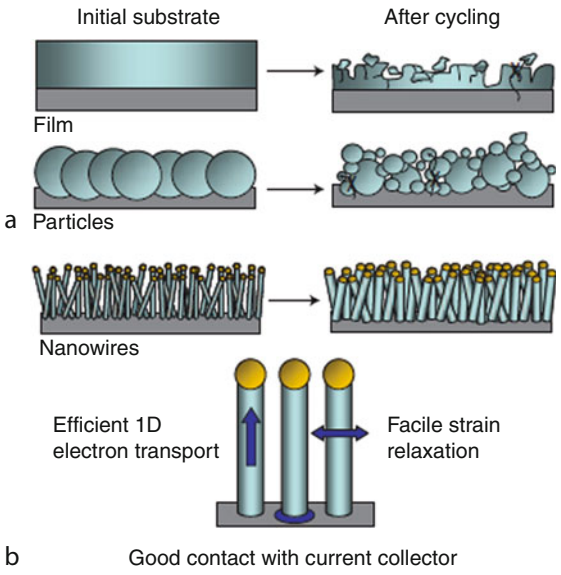

Fig. 15.7 Schematic of morphological changes of silicon during cycling. (**a**) The volume of silicon anodes changes by about 400% during cycling. (**b**) SiNWs do not disintegrate or break into smaller particles after cycling. This SiNW anode design has each nanowire connecting with the current collector (Reprinted with permission from Chan et al. [80]. Copyright 2008)

dispersed graphene/graphite matrix then buffers the volume expansion/contraction of silicon particles during repeated alloying and de-alloying with lithium [78, 79]. Specific capacities exceeding 1,500 mAh/g after 200 cycles with a capacity fading rate of less than 0.5% per cycle have been achieved using this approach.

One-Dimensional Silicon Nanowires

The previous section clearly established that the morphology, size, and structure of the silicon phase can have a dramatic effect on the ultimate performance and stability of a silicon-based anode. Figure 15.7 graphically depicts observed morphological changes that occur in thin-film silicon during electrochemical cycling when different starting morphologies are used. The rod-like microstructures formed during initial charge processes of silicon films (Fig. 15.6) suggest that one-dimensional geometries (such as silicon nanowires [SiNWs]) may provide a stable structure that could be synthesized from a more viable manufacturing route. In 2008, Chan et al. [80] prepared SiNWs (diameter $<$ 100 nm) using a CVD method based on the vapor-liquid-solid mechanism using silane gas as the silicon source, gold as the catalyst with stainless steel substrates. The one-dimensional SiNWs grown directly on the stainless steel current collector had a measured capacity of 4,277 mAh/g (based on the weight of silicon) during the first discharging process; this capacity is essentially the theoretical value for silicon within the experimental error. In subsequent cycles, the SiNWs maintained a charge/discharge capacity of 75% of the initial capacity, with little fading during cycling. The shortened lithium transport distances in the silicon nanostructure and

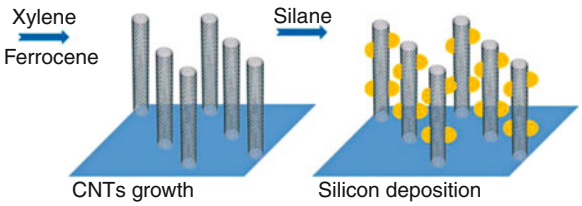

Fig. 15.8 Schematic diagram depicting the fabrication of silicon/carbon hybrid nanostructures using a liquid-injection CVD process to grow the initial vertically aligned CNTs, followed by the subsequent deposition of silicon (Reprinted with permission from Wang and Kumta [18]. Copyright 2010 American Chemical Society)

the low-resistance electrical connection to the current collector also led to an excellent rate capability (>2,100 mAh/g at 1C). While sufficient for concept demonstration and material design, the large-scale application of SiNWs grown directly on a current collector (foil) is still limited by the high production cost of SiNWs and the small weight ratio of active material to inactive material in the complete anode (which includes the substrate/current collector).

Several other approaches have been used to grow silicon-based nanowires. For example, Yu et al. [81] prepared SiNWs on silicon wafers using the solid-liquid-solid (SLS) mechanism. Kolb et al. [82] prepared silicon-based nanowires by evaporating silicon monoxide (SiO) in an inert gas atmosphere using a gold-coated silicon wafer as a substrate. Chang et al. [83] reported growth of silicon-based nanowires by heat treatment of an iron-catalyst–coated silicon nanopowder at 980°C. However, no electrochemical performances of these silicon-based nanowires were reported. Recently, Zhang et al. [84] prepared free-standing silicon-based nanowires from commercial silicon powders in a three-dimensional manner rather than on the surface of the substrate (i.e., two-dimensional growth). A vapor-induced SLS mechanism was proposed to explain the observed growth of the resulting multicomponent nanowires from solid-powder sources. The composition, morphology, crystal structure, and electrochemical performance of the nanowires also were investigated.

In addition to growth of SiNWs, one-dimensional composite structures prepared by vacuum deposition of silicon clusters on CNTs also have been investigated. Hybrid silicon/carbon nanotube one-dimensional nanostructures were synthesized using a two-step CVD process (see Fig. 15.8) [18]. The spaces between the CNTs, formed through controlled nucleation in the first deposition step, allow for subsequent penetration of silane gas and a homogenous deposition of silicon clusters on the surfaces of the CNTs during the second CVD deposition step. The hybrid silicon/CNTs exhibit a high reversible capacity of 2,000 mAh/g with a 0.15% capacity loss per cycle over 25 cycles. When compared with commercially available silicon particles, in situ prepared silicon by CVD always has a smaller irreversible capacity loss in the first cycle. This may be related to the reduced amount of SiO_x on the surface of the silicon particles which usually traps lithium in

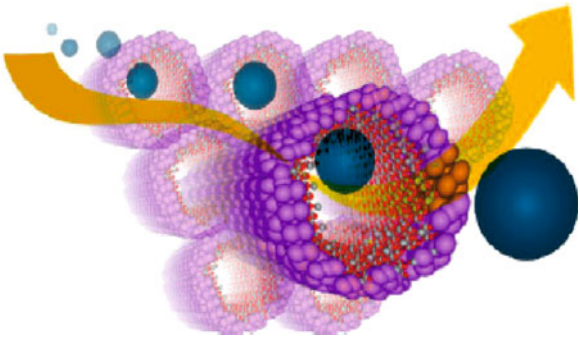

Fig. 15.9 Schematic diagram of the lithium-ion pathway in silicon nanotubes (Reprinted with permission from Park et al. [21]. Copyright 2009 American Chemical Society)

the form of Li_2O and silicon in the first cycle. Coating silicon clusters on graphite nanofibers may also provide promising improvements in the cycling performance of silicon-based anodes.

Three-Dimensional Nanostructured Silicon Anodes

In addition to one-dimensional and two-dimensional silicon anodes, several forms of three-dimensional nanostructured silicon have been explored. For example, silicon nanotubes (Fig. 15.9) were investigated by Cho et al. [21] as an anode material for lithium-ion batteries. Both interior and exterior surfaces of the nanotubes are accessible to the electrolyte and lithium ions. Through carbon coating, a stable solid electrolyte interface (SEI) was generated on the inner and outer surfaces of the silicon nanotubes. These silicon/carbon assemblies showed a reversible capacity as high as 3,247 mAh/g (based on the weight of silicon) and good capacity retention.

Three-dimensional porous silicon was recently investigated as a high-performance anode material for lithium-ion batteries [85]. The three-dimensional porous silicon particles with in situ coated carbon on the surface contained many "octopus foot"-like voids as shown in Fig. 15.10. This highly porous, interconnected structure not only facilitates the transport of lithium ions but also significantly alleviates the detrimental effects of volume expansion and shrinkage. At a 3C rate (1C rate = 2,000 mA/g or 40 mA/cm^2), a discharge capacity of 2,158 mAh/g (based on the weight of silicon) with a 72% capacity retention was obtained after 100 cycles. Earlier reports on nanoporous silicon/carbon composites showed similar cycling stability [86]. A reversible capacity of 700 mAh/g based on the total weight of nanoporous silicon/graphite/carbon electrode was obtained with negligible capacity loss up to 120 cycles. Commercially available micrometer-sized silicon particles with nanoporous surface structures (Fig. 15.11) have also been investigated. Stable cycling behavior could be achieved if CVD carbon coatings were applied to individual silicon particles and an elastic carbon additive was used

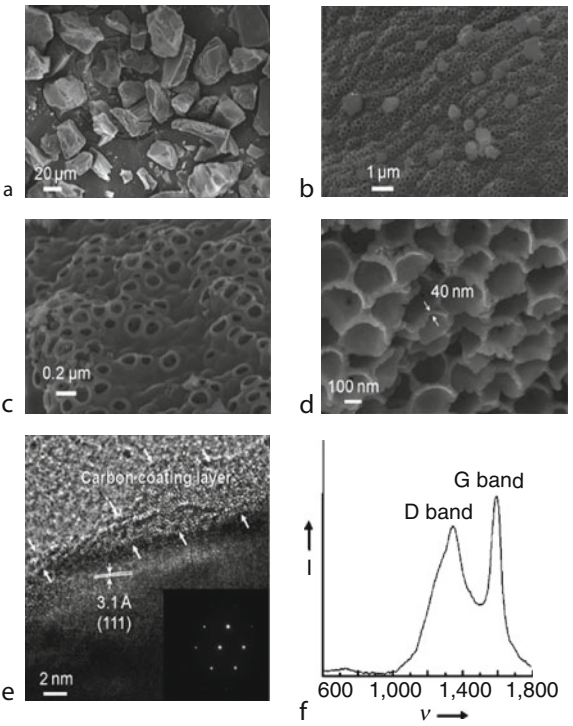

Fig. 15.10 (**a**), (**b**), (**c**), (**d**) SEM images of the three-dimensional porous c-silicon particles after etching ([**d**] is the cross-sectioned image of [**e**]). (**e**) TEM image of the cross-sectioned, three-dimensional porous c-silicon particle (the inset shows a selected area diffraction pattern. (**f**) Raman spectrum of three-dimensional porous c-silicon particles after etching. I = intensity (Reproduced with permission from Kim et al. [85]. Copyright Wiley-VCH Verlag GmbH & Co. KGaA)

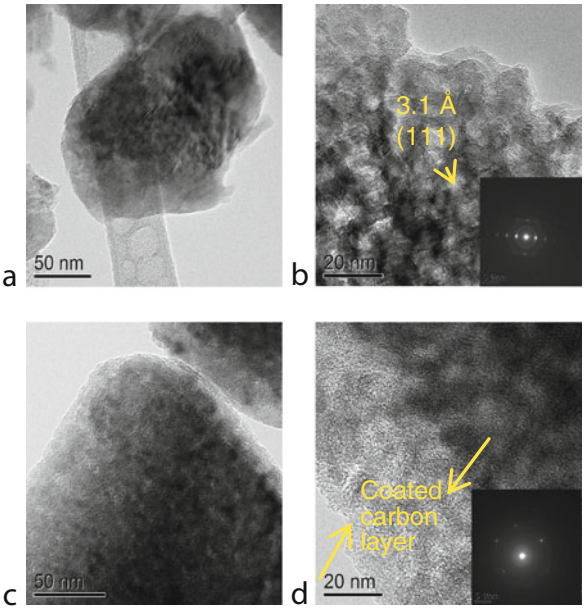

Fig. 15.11 (**a**) and (**b**) TEM images of porous silicon at different magnifications before carbon coating. (**c**) and (**d**) TEM images of silicon at different magnifications after carbon coating using CVD [1] (Reprinted with permission from Xiao et al. [87]. Copyright 2010 The Electrochemical Society)

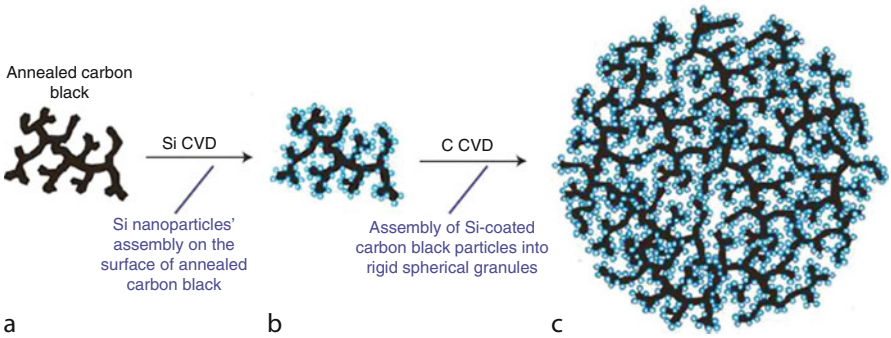

Fig 15.12 Schematic of silicon/carbon nanocomposite granule formation through hierarchical bottom-up assembly. (**a**–**c**). Annealed carbon-black dendritic particles (**a**) are coated by silicon nanoparticles (**b**) and then assembled into rigid spheres with open interconnected internal channels during C deposition (**c**) (Reprinted with permission from Magasinski et al. [89]. Copyright 2010)

to improve interparticle contact in the anode [87]. Nest-like silicon structures also are reported to have better electrochemical performance than that of coil-like silicon nanospheres, probably through a mechanism similar to that used to form three-dimensional nanostructured silicon [88].

To further improve the mechanical and electrical stability of silicon-based anodes, a hierarchical bottom-up approach (Fig. 15.12) was successfully utilized to develop a three-dimensional nanostructured silicon/carbon porous composite [89]. The existence of pores in the composite granules provides sufficient space to accommodate silicon expansion during lithium insertion. CVD deposition of silicon clusters (Fig. 15.12b) avoids formation of SiO_x, thus reducing the first cycle, irreversible capacity. A high specific capacity of ~1,950 mAh/g (C/20 rate) based on the total weight of the silicon/carbon composite was reported. In addition, the composite anodes had negligible capacity fade after 100 cycles at 1C rate and excellent rate capability (870 mAh/g at 8C rate).

Effect of Binder on the Performance of Silicon-Based Anodes

Sodium Carboxylmethylcellulose–Based Binder

Polyvinylidenedifluoride (PVDF) has been used widely as the binder for graphite-based anodes in lithium-ion batteries. However, silicon-based anodes with a PVDF-based binder exhibit poor cyclability. Therefore, significant efforts have been made during the last 10 years to develop new binders that can improve the performance of silicon-based anodes. Chen et al. [90] first reported that a poly(vinylidene fluoride-–tetrafluoroethylene–propylene)-based elastomeric binder system kept the capacity of the amorphous $Si_{0.6}Sn_{0.4}$ alloy at around 800 mAh/g for 40 cycles, while the

PVDF binder only showed ~490 mAh/g at the thirtieth cycle. Considering the fact that breakage elongation of the new elastomeric binder is much larger than that for PVDF [91, 92], the elastomeric binder could improve the cycling performance of a silicon-based alloy electrode.

In recent years, several new materials have been developed as effective binders for silicon-based anodes. Liu et al. [93] reported that the cycle life of silicon-based electrodes (either with or without carbon coating) was significantly improved by using a modified elastomeric binder containing styrene-butadiene-rubber (SBR) and sodium carboxylmethylcellulose (SCMC). When an SBR-SCMC mixture binder was used, the anodes with bare silicon and carbon-coated silicon exhibited a capacity of 600 mAh/g and 1,000 mAh/g, respectively at >50 cycles. In comparison, the capacity of a silicon electrode with a PVDF binder quickly decreased to several mAh/g after eight cycles. This is because the SBR-SCMC binder has a lower elastic modulus, a larger maximum elongation, better adhesion to the copper current collector, and much less solvent absorption in organic carbonate electrolytes. Several other research groups [46, 94–97] also have reported improved performance on silicon/carbon composite electrodes using an SBR-SCMC mixture binder over PVDF binder (sometimes combined with SBR [98]). Although a recent report shows that a thermally annealed PVDF can reconstruct the compact morphology of the electrode, the long-term cycling stability of a silicon electrode using an annealed PVDF binder is still inferior to that using CMC as the binder [99]. Li et al. [94] showed that the cycling performance of the crystalline silicon-powder electrode was improved further by using only SCMC as the binder over the SBR-SCMC mixture binder. Li et al. suggests that the stiff SCMC polymer might restrict the volume change of the silicon particles to only about 100% and also might modify the silicon particle surface. Thus, the binding mechanism of SCMC for a silicon electrode should be different from that of PVDF.

Hochgatterer et al. [100] reported that the improved long-term cycling behavior in an anode with an SCMC binder can be attributed to the formation of a covalent chemical bond between the SCMC binder and the silicon particles. SCMC exhibits a porous scaffold structure with cavities or pores that allow the silicon particles to expand without severe deformation of the electrode. Therefore, the cycle stability can be improved. Lestrie et al. [96] suggested that the efficiency of SCMC was likely attributed to the formation of an efficient conductive silicon/carbon-SCMC network because of its extended conformation in solution. Moreover, the silicon/carbon-SCMC electrode prepared at pH 3 showed prolonged cyclability improvement, which probably resulted from the physical cross-linking of the SCMC chains in the acid solution. Guo and Wang [101] recently reported a polymer scaffold structure based on an SCMC binder for a silicon electrode. The SCMC scaffold-based silicon electrode had much higher surface area and total pore volume but a reduced mean pore diameter than the SCMC-based silicon electrode prepared using a conventional method. Therefore, silicon nanoparticle electrodes with a SCMC scaffold binder structure could accommodate greater volume changes from the silicon, enhance lithium-ion transport in the electrodes, and improve the electrochemical reaction kinetics. In addition, high energy and power densities and

superb cycle stability were achieved for porous SCMC, scaffold-based silicon electrodes. After 150 cycles at a rate of 250 mA/g, the anode capacity remained at 1,685 mAh/g based on the weight of silicon. The improved rate performance of silicon is attributed to the SCMC scaffold, which facilitates lithium-ion transport in the porous electrode and accelerates the charge transfer reaction kinetics [101].

Although the binding mechanism of SCMC in silicon electrodes is unclear, the significant performance improvements observed drives efforts to optimize SCMC/silicon-based electrodes. In fact, some researchers believe that the binder plays a more important role than the nanostructure of the silicon particles on the performance of silicon-based anodes. Beattie et al. [102] reported that silicon-based electrodes with a relatively low silicon content (20–34 wt.%) and a high SCMC content (33–56 wt.%) had large capacities (660 mAh/g) for hundreds of cycles. They believed that, if an appropriate binder was used with silicon electrodes, no special electrode processing or cycling procedures were required to achieve high capacities with good cyclability.

Other Binders

In addition to SCMC, several other polymeric binders have been developed for silicon-based anodes in recent years. Zheng et al. [103] reported that a nanoporous silicon/graphite/carbon composite electrode containing polyacrylic latex LA132 binder (10 wt.%) exhibited a reversible capacity of 650 mAh/g after 200 cycles with negligible capacity loss. Chen et al. [104] reported a significant cycling-performance enhancement for silicon/carbon composite electrodes using an acrylic adhesive (polyacrylic latex, LA132) and a modified acrylic adhesive with SCMC. The capacity retentions of the silicon/carbon composite electrodes were 79% and 90% after 50 cycles, respectively, while the silicon/carbon composite electrode with PVDF retained only 67% of its initial capacity. This was ascribed to improved adhesion between the coating and the copper current collector, as well as reduced solvent absorption of the electrolyte solvent than with PVDF. Polyamide imide (PAI) also can significantly improve the initial coulombic efficiency of a silicon-based anode because of PAI's excellent mechanical properties and ease of processing, which maintains the stability of the electrical-conducting network during charge/discharge processes [105].

Recently, Liu et al. [106] reported on conductive polymers used as both the binder and the conductive matrix. The electronic conductivity of the reported binder increases during the lithium-insertion process. Stable cycling above ~1,200 mAh/g (based on silicon) was reported for the silicon-based anode using these binders. The cycling stability of silicon improved significantly, especially within the reduced electrochemical window (0.17–0.9 V) [107]. However, the initial irreversible capacity loss in these anodes still requires further improvement (i.e., reduction) before these silicon-based anodes can be used in a full cell. Cámer et al. [108] reported that silicon-composite electrodes with very good electrochemical performance could be prepared by simply mixing appropriate amounts of nanosized silicon and cellulose

fibers without including conductive carbon and other binders. A silicon/carbon cellulose composite electrode at a weight ratio of 34:66 exhibited very good cycling performance. A specific capacity of ~1,400 mAh/g after 50 cycles was obtained, compared to only 400 mAh/g for an electrode made from pure silicon. Cámer et al. believe that the improved performance resulted from mitigation of the large volume changes of silicon particles during lithium insertion and de-insertion and the retention of connectivity between particles by the binder-like fibers.

Effect of Electrolytes on the Performance of Silicon-Based Anodes

The effect of nonaqueous electrolytes and additives on the performance of silicon electrodes has not been systematically investigated. The electrolytes used in the investigation of silicon-based electrodes were mainly adopted from electrolytes for graphite-based lithium-ion batteries (i.e., $LiPF_6$ in carbonate mixtures of EC and DMC, ethyl methyl carbonate [EMC] or diethyl carbonate [DEC]). Alternative electrolytes used in the study of silicon-based anodes include (1) adding SEI formation additives into the regular electrolytes of $LiPF_6$ in carbonates, (2) using different lithium salts, (3) using different solvent systems, (4) using ionic-liquid-based electrolytes, (5) using polymer electrolytes, and (6) using solid-state electrolytes. The effects of these electrolytes on the performance of a silicon-based electrode are reviewed in this section.

SEI Formation Additives

Formation of the SEI layer plays an important role on the cycling stability of silicon-based anodes. Kulova and Skundin [109] reported a method used to preform the SEI layer on an electrode surface (prior to initial cathodic polarization) by direct contact of silicon and lithium metal in the electrolyte. The electrolyte was 1-M $LiClO_4$ in a mixture of propylene carbonate (PC) and dimethoxyethane. This method effectively reduced the irreversible capacity of the amorphous silicon electrode. Pretreatment of nanometer-sized silicon in ethanol also can form functionalized surfaces on the silicon particles that improve adhesion of silicon-based electrodes. A stable capacity of 2,500 mAh/g after 25 cycles has been reported for ethanol-treated silicon electrodes [110].

Several electrolyte additives have been used to form stable SEI layers and improve cyclability of silicon anodes. Doh et al. [111] used 5% 4-fluoroethylene carbonate (FEC) in the electrolyte of 1.0-M $LiPF_6$ in EC/DMC/EMC/PC at a volume ratio of 4:3:3:1 when investigating silicon/carbon composites formed by polyaniline carbonization. They found that the addition of FEC to the electrolyte increased the initial discharge capacity of the silicon/carbon composites when compared with the electrolyte without FEC. Choi et al. [112] reported that the

discharge capacity retention and coulombic efficiency of a silicon thin-film electrode could be significantly improved by adding 3% of FEC into the electrolyte of 1.3-M $LiPF_6$ in EC/DEC (3:7 by volume). They used SEM and X-ray photoelectron spectroscopy (XPS) to investigate the surface morphology and chemical composition of the SEI layers formed on the surface of the silicon thin-film electrode after cycling. The SEI layer structure formed in the FEC-containing electrolyte was much smoother and more stable than those formed in electrolytes that did not contain the FEC additive. Chen et al. [113] investigated the effect of vinylene carbonate (VC) as an electrolyte additive on the electrochemical performance of a silicon thin-film anode. They found that the cycle performance and efficiency of the silicon thin-film anode were significantly enhanced with the addition of 1% VC into the electrolyte of 1-M $LiPF_6$ in EC/DMC. The capacity of the silicon thin film shows minimal fade after 500 cycles, which was attributed to the advanced properties of the SEI layer formed during the initial cycles. Actually, in both VC-containing and VC-free electrolytes, the major components of the SEI layer on the silicon thin-film anode were quite similar and primarily consist of lithium salts (e.g., $ROCO_2Li$, Li_2CO_3, LiF), polycarbonates, and silicon oxide formed through the reaction of lithiated silicon with permeated electrolyte. However, the morphology of the SEI layer was smoother and more uniform in VC-containing electrolytes than in VC-free electrolytes. The impedance of the SEI layer in VC-containing electrolytes did not change significantly upon cycling because of the presence of VC-reduced products and less LiF content in the SEI layer, which led to better properties of the SEI layer. However, the impedance of the SEI layer in a VC-free electrolyte increased constantly upon cycling because of the increasing thickness and high LiF content in the SEI layer, resulting in increased electrode polarization and degradation in the cycling performance of the silicon thin-film anode.

Han et al. [114] studied the effect of succinic anhydride (SA) as an electrolyte additive on the electrochemical performances of a silicon thin-film electrode. They found that addition of a small amount (3 wt.%) of SA into the electrolyte of 1-M $LiPF_6$ in EC/DEC could significantly enhance the capacity retention and coulombic efficiency of the silicon electrode. SA also prevented decomposition of the $LiPF_6$ salt, and the SEI layer contained higher levels of hydrocarbon and Li_2CO_3 on the silicon surface. Modification to the SEI layer by SA was probably the primary factor for the enhanced performance of the silicon thin-film electrode. Baggetto et al. [115] used a poly-silicon thin film as the active anode material and cycled the poly-silicon anodes in one solid and two liquid electrolytes to investigate the thermodynamic and kinetic properties of the anodes and the growth of SEI layers on top of poly-silicon anodes. They studied the electrochemical and material characteristics of a potential planar anode stack (active anode material/barrier layer/silicon substrate) for all-solid-state, three-dimensional, integrated batteries. The solid-state electrolyte was amorphous lithium phosphorus oxynitride (LiPON), and the two liquid electrolytes were 1-M $LiPF_6$ in EC/DEC and 1-M $LiClO_4$ in PC. The silicon electrodes cycled in the two liquid electrolytes showed stable storage capacities up to about 30 or 40 cycles, respectively, then the capacities decreased sharply. When the inorganic solid-state electrolyte LiPON was used

to overcoat the silicon, no degradation in capacity was observed for 60 cycles. Cross-sectional SEM analysis revealed thick, porous SEI layer formation in the case of $LiPF_6$ and $LiClO_4$ based electrolytes. The silicon layer was almost invisible, and it seemed to be "dissolved" within the SEI layer, implying that the active silicon clusters slowly became electronically isolated resulting in the loss of reversible capacity. In contrast, the silicon covered by a LiPON layer had no visible SEI layer formation and improved cycle life over cells that were LiPON-free.

Arie et al. [116] investigated the electrochemical characteristics of phosphorus- and boron-doped silicon thin-film (n-type and p-type silicon) anodes integrated with a solid polymer electrolyte in lithium-polymer batteries. The doped silicon electrodes showed enhanced discharge capacity and coulombic efficiency over the un-doped silicon electrode, and the phosphorus-doped, n-type silicon electrode showed the most stable cyclic performance after 40 cycles with a reversible specific capacity of about 2,500 mAh/g. The improved electrochemical performance of the doped silicon electrode was mainly due to enhancement of its electrical and lithium-ion conductivities and stable SEI layer formation on the surface of the electrode. In the case of the un-doped silicon electrode, an unstable surface layer formed on the electrode surface, and the interfacial impedance was relatively high, resulting in high electrode polarization and poor cycling performance.

Alternative Solvents and Salts

Inose et al. [117] studied the influence of glyme-based electrolyte solutions on charge-discharge properties of two silicon-based anodes prepared from (1) a silicon/carbon mixture and (2) a mixture of a silicon-SiO_2-carbon composite and carbon (Si-C/C). After glymes of poly(ethylene glycol) dimethyl ethers [$(CH_3O(CH_2CH_2O)_nCH_3$, $n = 1, 2, 3$ and 4)] were added into an electrolyte solution of 1 M $LiPF_6$ in EC and EMC (3:7 by vol), the discharge capacity tended to increase relative to electrolytes without glyme additions. Carbon coating of the silicon particles in the Si-C/C electrode improved cycle life when compared to the silicon/carbon electrode. Physical breakdown of the electrode was suppressed by the thin carbon surface layer, and reactivity of electrolyte toward lithium metal also was reduced. They also found that the discharge capacity of the silicon/carbon electrode was dependent on the reduction potential of the glymes, while the discharge capacity of the Si-C/C electrode depended on electrolyte conductivity.

Choi et al. [118] compared the effect of two different lithium salts on the cycling performance of a 200-nm silicon thin-film electrode. The electrolytes tested were 1.3-M $LiPF_6$ in EC/DEC (3:7 by vol) and 0.7-M lithium bis(oxalato) borate (LiBOB) in the same solvent mixture. They found that the LiBOB-based electrolyte markedly improved the discharge capacity retention of the lithium-silicon half-cell, over the $LiPF_6$-based electrolyte. The surface layer on the silicon electrode in the LiBOB-based electrolyte was less porous and effectively limited the formation of electrochemically inactive silicon phases. The capacity fading of the lithium-silicon

half-cell was strongly related to the physical morphology of the silicon surface and also to the formation of inactive silicon phases in the surface layer.

Ionic liquids have also been studied as possible electrolytes in silicon-based anode cells. Lux et al. [119] evaluated the use of N-butyl-N-methylpyrrolidinium bis (trifluoromethylsulfonyl)imide (PYR14TFSI) as a solvent for silicon electrodes at room temperature. The electrolyte contained 0.3-M lithium bis(trifluoromethylsulfonyl)imide ($LiN(SO_2CF_3)_2$, LiTFSI) in PYR14TFSI + 5 wt.% VC. The performance of silicon electrodes in PYR14TFSI-based electrolytes was comparable with that of the same electrodes in more conventional organic solvent-based electrolytes. The degree of affinity between ionic liquids and active materials was suggested as an important parameter for the selection and use of ionic liquids in lithium batteries.

Full Cells Containing Silicon-Based Anodes

To fully evaluate the efficacy of silicon-based anodes, testing in a full-cell configuration against a lithium intercalation cathode, such as $LiCoO_2$, is required because of possible detrimental interactions between the cathode and anode (through electrolyte as the media), as was discovered in the case of graphite/$LiMn_2O_4$. In addition, the management of volume change in the complete cells is not a trivial challenge for silicon-based cells where the anode exhibits large volume variations during cycling. Nonetheless, studies of electrochemical performance for silicon-anode-based full batteries are rare, possibly because of the poor cycling performance of these anodes, which remains a hurdle to practical application of the technology.

Cui et al. [120] reported a full-cell test using a $LiCoO_2$ cathode and carbon-silicon core-shell nanowire anode. This anode has about 10 times the specific capacity of the cathode and, therefore, a mass loading approximately 10 times lower than that of the cathode. The full cell operated at ~3.3 V with a sloping voltage profile and a fast fade of ~0.7% per cycle. The same group also reported full battery performance of the silicon nanowire anode and sulfur-based cathode pair [121]. Although the voltage profile of the full-cell test revealed large overpotentials because of poor electrical conductivity of the Li_2S cathode, the specific energy density of the battery was reported to be approximately four times higher than the current $LiCoO_2$/graphite-based, lithium-ion battery mostly because of the high specific capacity of the sulfur cathode. High-voltage $LiNi_{0.5}Mn_{1.5}O_4$ also has been paired with silicon nanoparticles to form a full-cell battery [122]. The cycling performance at increased operating voltage resulted in higher specific capacity than a conventional $LiCoO_2$/graphite-based commercial battery. However, the cycling stability of this battery is still problematic. There also are reports of thin-film batteries using amorphous silicon anodes paired with $LiMn_2O_4$ [123] or $LiCoO_2$ cathodes [124–126] with better cyclability than the similar bulk batteries, but

large-scale manufacturing of thin-film batteries is hindered by the high manufacturing cost of these materials.

Future Directions

Although the silicon-based anode has great potential to significantly improve the capacity of lithium-ion batteries, there are still many obstacles that prevent its practical application. Long-term cycling stability remains the foremost challenge facing the battery research community. The cyclability of full cells using silicon-based anodes is complicated by multiple factors, such as diffusion-induced stress and fracture [127], loss of electrical contact among silicon particles and between silicon and current collector, and the breakdown of SEI layers during volume expansion/contraction processes. A detailed study of the design and engineering of a full cell with a silicon-based anode still needs to be conducted after a stable silicon-based anode structure is developed. Critical research remaining in this area includes, but is not limited to, the following:

- Further understanding of the effect of SEI formation on the cyclability of silicon-based anodes. Electrolytes and additives that can produce a stable SEI layer need to be developed. In situ SEM of working electrochemical test cells could be a very useful tool to directly observe the formation and evolution of SEI layers.
- The effect of particle size and the mechanical stability of silicon particles need to be understood. A theoretical model needs to be developed to find the critical dimension at which silicon particles are stable under long-term expansion/shrinking cycles.
- A good binder and conductive matrix (such as carbon) need to be developed. They should provide flexible but stable electrical contacts among silicon particles and between particles and the current collector under repeated volume changes during charge/discharge processes. The specific capacity of the complete anode (including the silicon, binder, and conductive matrix) needs further optimization. An acceptable balance between the specific capacity and the long-term stability of the anode also is needed. Considering the fact that the specific capacity of state-of-the-art cathodes is between ~140 mAh/g and 200 mAh/g, Kasavajjula et al. [24] suggest that improvement in the total capacity of an 18,650 cell is negligible after the anode specific capacity reaches more than 1,200 mAh/g if other components of the batteries remain unchanged. Based on this analysis, a specific capacity of ~1,200 mAh/g for the complete anode with a loading of 5–10 mg/cm^2 would be a reasonable technical target. Improvement in cycling stability remains the primary challenge for silicon-based anodes.
- The performance of full cells needs to be studied and optimized. Parameters to be optimized include cell geometry, anode and cathode balancing, accommodation of volume expansion, and electrolyte/additive selection.

Last, it should be recognized that the overall effect of the high-capacity anode on the performance of lithium-ion batteries is limited primarily because the anode only occupies a relatively small portion of the total weight (15–20%) and volume of the lithium-ion battery [128]. An anode with infinite specific capacity (or zero weight) could only lead to less than a 20% reduction in the total weight of the system, if other components of the battery remain the same. Many factors affect the total specific capacity and weight/volume of a full battery, such as the specific capacities of the anode and cathode, electrolyte, separator, current collectors, and case. Therefore, significant improvements in both the anode and the cathode, as well as other battery components, must be achieved to realize the goal of producing widely applied, high-energy batteries.

Bibliography

1. Boukamp BA, Lesh GC, Huggins RA (1981) All-solid lithium electrodes with mixed-conductor matrix. J Electrochem Soc 128:725–729
2. Dey AN (1971) Electrochemical, alloying of lithium in organic electrolytes. J Electrochem Soc 118:1547–1549
3. Tirado JL (2003) Inorganic, materials for the negative electrode of lithium-ion batteries: state-of-the-art and future prospects. Mater Sci Eng R Rep 40:103–136
4. Winter M, Besenhard JO (1999) Electrochemical lithiation of tin and tin-based intermetallics and composites. Electrochim Acta 45:31–50
5. Kim I-S (2003) Synthesis, structure and properties of electrochemically active nanocomposites. Ph.D thesis, Carnegie Mellon University
6. Sharma RA, Seefurth RN (1976) Thermodynamic properties of the lithium-silicon system. J Electrochem Soc 123:1763–1768
7. van der Marel C, Vinke GJB, van der Lugt W (1985) The phase diagram of the system lithium-silicon. Solid State Commun 54:917–919
8. Lai S-C (1976) Solid lithium-silicon electrode. J Electrochem Soc 123:1196–1197
9. Li H et al (2000) The crystal structural evolution of nano-Si anode caused by lithium insertion and extraction at room temperature. Solid State Ionics 135:181–191
10. Limthongkul P, Jang Y-I, Dudney NJ, Chiang Y-M (2003) Electrochemically-driven solid-state amorphization in lithium-silicon alloys and implications for lithium storage. Acta Mater 51:1103–1113
11. Limthongkul P, Jang Y-I, Dudney NJ, Chiang Y-M (2003) Electrochemically-driven solid-state amorphization in lithium-metal anodes. J Power Sources 119–121:604–609
12. Maranchi JP, Hepp AF, Kumta PN (2003) High capacity reversible silicon thin film anodes lithium ion batteries. Electrochem Solid-State Lett 6:A198–A201
13. Ryu JH, Kim JW, Sung Y-E, Oh SM (2004) Failure modes of silicon powder negative electrode in lithium secondary batteries. Electrochem Solid-State Lett 7:A306–A309
14. Li J, Dahn JR (2007) An in situ x-ray diffraction study of the reaction of Li with crystalline Si. J Electrochem Soc 154:A156–A161
15. Obrovac MN, Christensen L (2004) Structural changes in silicon anodes during lithium insertion/extraction. Electrochem Solid-State Lett 7:A93–A96
16. Hatchard TD, Dahn JR (2004) In situ XRD and electrochemical study of the reaction of lithium with amorphous silicon. J Electrochem Soc 151:A838–A842
17. Datta MK, Kumta PN (2009) In situ electrochemical synthesis of lithiated silicon-carbon based composites anode materials for lithium ion batteries. J Power Sources 194:1043–1052

18. Wang W, Kumta PN (2010) Nanostructured hybrid silicon/carbon nanotube heterostructures: reversible high-capacity lithium-ion anodes. ACS Nano 4:2233–2241
19. Obrovac MN, Krause LJ (2007) Reversible cycling of crystalline silicon powder. J Electrochem Soc 154:A103–A108
20. Beaulieu LY, Eberman KW, Turner RL, Krause LJ, Dahn JR (2001) Colossal reversible volume changes in lithium alloys. Electrochem Solid-State Lett 4:A137–A140
21. Park MH et al (2009) Silicon nanotube battery anodes. Nano Lett 9:3844–3847
22. Datta MK, Kumta PN (2006) Silicon and carbon based composite anodes for lithium ion batteries. J Power Sources 158:557–563
23. Sandia National Laboratories. Sandia National Laboratories News Releases. Sandia National Laboratories, Livermore, CA, 6 March 2003
24. Kasavajjula U, Wang C, Appleby AJ (2007) Nano- and bulk-silicon-based insertion anodes for lithium-ion secondary cells. J Power Sources 163:1003–1039
25. Larcher D et al (2007) Recent findings and prospects in the field of pure metals as negative electrodes for Li-ion batteries. J Mater Chem 17:3759–3772
26. Timmons A et al (2007) Studies of Si[sub 1 – x]C[sub x] electrode materials prepared by high-energy mechanical milling and combinatorial sputter deposition. J Electrochem Soc 154:A865–A874
27. Huggins RA (1999) Lithium, alloy negative electrodes. J Power Sources 81–82:13–19
28. Mao O et al (1999) Active/inactive nanocomposites as anodes for Li-ion batteries. Electrochem Solid-State Lett 2:3–5
29. Weydanz WJ, Wohlfahrt-Mehrens M, Huggins RA (1999) A room temperature study of the binary lithium-silicon and the ternary lithium-chromium-silicon system for use in rechargeable lithium batteries. J Power Sources 81–82:237–242
30. Courtney IA, McKinnon WR, Dahn JR (1999) On the aggregation of tin in SnO composite glasses caused by the reversible reaction with lithium. J Electrochem Soc 146:59–68
31. Mayo MJ (1997) High, and low temperature superplasticity in nanocrystalline materials. Nanostruct Mater 9:717–726
32. Wang W (2009) Silicon Based Nanocomposites as Lithium-ion Battery Anodes. PhD dissertation, Carnegie Mellon University
33. Idota Y, Kubota T, Matsufuji A, Maekawa Y, Miyasaka T (1997) Tin-based amorphous oxide: a high-capacity lithium-ion-storage material. Science 276:1395–1397
34. Hwang S-M et al (2001) Lithium insertion in SiAg powders produced by mechanical alloying. Electrochem Solid-State Lett 4:A97–A100
35. Kim H, Choi J, Sohn H-J, Kang T (1999) The insertion mechanism of lithium into Mg[sub 2] Si anode material for Li-ion batteries. J Electrochem Soc 146:4401–4405
36. Kim I-S, Kumta PN, Blomgren GE (2000) Si/TiN nanocomposites novel anode materials for Li-ion batteries. Electrochem Solid-State Lett 3:493–496
37. Kim I-S, Blomgren GE, Kumta PN (2004) Si-SiC nanocomposite anodes synthesized using high-energy mechanical milling. J Power Sources 130:275–280
38. Kim I-S, Blomgren GE, Kumta PN (2003) Nanostructured Si/TiB_2 composite anodes for Li-ion batteries. Electrochem Solid-State Lett 6:A157–A161
39. Wang CS, Wu GT, Zhang XB, Qi ZF, Li WZ (1998) Lithium insertion in carbon-silicon composite materials produced by mechanical milling. J Electrochem Soc 145:2751–2758
40. Gross KJ, Wang JCF, Roberts GA (2004) Synthesis of carbon/silicon composites. US Patent 2004/137,327 (2004)
41. Kim I-S, Kumta PN (2004) High capacity Si/C nanocomposite anodes for Li-ion batteries. J Power Sources 136:145–149
42. Wilson AM, Reimers JN, Fuller EW, Dahn JR (1994) Lithium insertion in pyrolyzed siloxane polymers. Solid State Ionics 74:249–254
43. Yang J et al (2003) Si/C composites for high capacity lithium storage materials. Electrochem Solid-State Lett 6:A154–A156

44. Xie J, Cao GS, Zhao XB (2004) Electrochemical performances of Si-coated MCMB as anode material in lithium-ion cells. Mater Chem Phys 88:295–299
45. Holzapfel M et al (2005) Chemical vapor deposited silicon/graphite compound material as negative electrode for lithium-ion batteries. Electrochem Solid-State Lett 8:A516–A520
46. Holzapfel M, Buqa H, Scheifele W, Novak P, Petrat F-M (2005) A new type of nano-sized silicon/carbon composite electrode for reversible lithium insertion. Chem Commun 1566–1568
47. Dimov N, Fukuda K, Umeno T, Kugino S, Yoshio M (2003) Characterization of carbon-coated silicon: structural evolution and possible limitations. J Power Sources 114:88–95
48. Liu W-R et al (2005) Electrochemical characterizations on Si and C-coated Si particle electrodes for lithium-ion batteries. J Electrochem Soc 152:A1719–A1725
49. Yu M-F, Files BS, Arepalli S, Ruoff RS (2000) Tensile loading of ropes of single wall carbon nanotubes and their mechanical properties. Phys Rev Lett 84:5552
50. Krishnan A, Dujardin E, Ebbesen TW, Yianilos PN, Treacy MMJ (1998) Young's modulus of single-walled nanotubes. Phys Rev B 58:14013
51. Wong EW, Sheehan PE, Lieber CM (1997) Nanobeam mechanics: elasticity, strength, and toughness of nanorods and nanotubes. Science 277:1971–1975
52. Roche S (2000) Carbon nanotubes: exceptional mechanical and electronic properties. Ann Chim Sci Matériaux 25:529–532
53. Zhao Q, Nardelli MB, Bernholc J (2002) Ultimate strength of carbon nanotubes: a theoretical study. Phys Rev B 65:144105
54. Demczyk BG et al (2002) Direct mechanical measurement of the tensile strength and elastic modulus of multiwalled carbon nanotubes. Mater Sci Eng A 334:173–178
55. Thess A et al (1996) Crystalline ropes of metallic carbon nanotubes. Science 273:483–487
56. Yao Z, Kane CL, Dekker C (2000) High-field electrical transport in single-wall carbon nanotubes. Phys Rev Lett 84:2941
57. Frank S et al (1998) Carbon nanotube quantum resistors. Science 280:1744–1746
58. Shu J, Li H, Yang R, Shi Y, Huang X (2006) Cage-like carbon nanotubes/Si composite as anode material for lithium ion batteries. Electrochem Commun 8:51–54
59. Wang W, Kumta PN (2007) Reversible high capacity nanocomposite anodes of Si/C/SWNTs for rechargeable Li-ion batteries. J Power Sources 172:650–658
60. Si Q et al (2010) A high performance silicon/carbon composite anode with carbon nanofiber for lithium-ion batteries. J Power Sources 195:1720–1725
61. Guo JC, Sun A, Wang CS (2010) A porous silicon-carbon anode with high overall capacity on carbon fiber current collector. Electrochem Commun 12:981–984
62. Lee J et al (2009) Effect of randomly networked carbon nanotubes in silicon-based anodes for lithium-ion batteries. J Electrochem Soc 156:A905–A910
63. Jang S-M, Miyawaki J, Tsuji M, Mochida I, Yoon S-H (2009) The preparation of a novel Si-CNF composite as an effective anodic material for lithium-ion batteries. Carbon 47:3383–3391
64. Yang J, Winter M, Besenhard JO (1996) Small particle size multiphase Li-alloy anodes for lithium-ionbatteries. Solid State Ionics 90:281–287
65. Yang J, Takeda Y, Imanishi N, Ichikawa T, Yamamoto O (2000) SnSbx-based composite electrodes for lithium ion cells. Solid State Ionics 135:175–180
66. Yang J, Takeda Y, Imanishi N, Yamamoto O (1999) Ultrafine Sn and $SnSb_{0.14}$ Powders for lithium storage matrices in lithium-ion batteries. J Electrochem Society 146:4009–4013
67. Huggins R, Nix W (2000) Decrepitation model for capacity loss during cycling of alloys in rechargeable electrochemical systems. Solid State Ionics 6:57–63
68. Li H, Huang X, Chen L, Wu Z, Liang Y (1999) A high capacity nano-Si composite anode material for lithium rechargeable batteries. Electrochem Solid-State Lett 2:547–549
69. Beaulieu LY, Dahn JR (2000) The reaction of lithium with Sn-Mn-C intermetallics prepared by mechanical alloying. J Electrochem Soc 147:3237–3241
70. Gleiter H (1989) Nanocrystalline materials. Prog Mater Sci 33:223–315

71. Graetz J, Ahn CC, Yazami R, Fultz B (2003) Highly reversible lithium storage in nanostructured silicon. Electrochem Solid-State Lett 6:A194–A197
72. Maranchi JP, Hepp AF, Evans AG, Nuhfer NT, Kumta PN (2006) Interfacial properties of the a-Si/Cu:active–inactive thin-film anode system for lithium-ion batteries. J Electrochem Soc 153:A1246–A1253
73. Kim J-B, Lee H-Y, Lee K-S, Lim S-H, Lee S-M (2003) Fe/Si multi-layer thin film anodes for lithium rechargeable thin film batteries. Electrochem Commun 5:544–548
74. Kim Y-L et al (2003) Electrochemical characteristics of Co-Si alloy and multilayer films as anodes for lithium ion microbatteries. Electrochim Acta 48:2593–2597
75. Lee KL, Jung JY, Lee SW, Moon HS, Park JW (2004) Electrochemical characteristics of a-Si thin film anode for Li-ion rechargeable batteries. J Power Sources 129:270–274
76. Kim YL, Sun YK, Lee SM (2008) Enhanced electrochemical performance of silicon-based anode material by using current collector with modified surface morphology. Electrochim Acta 53:4500–4504
77. Yonezu I, Tarui H, Yoshimura S, Fujitani S, Nohma T (2004) Abstracts of the 12th International Meeting on Lithium Batteries, vol 58. Electrochemical Society, Nara, Japan, 2004
78. Lee JK, Smith KB, Hayner CM, Kung HH (2010) Silicon nanoparticles-graphene paper composites for Li ion battery anodes. Chem Commun 46:2025–2027
79. Chou SL et al (2010) Enhanced reversible lithium storage in a nanosize silicon/graphene composite. Electrochem Commun 2:303–306
80. Chan CK et al (2008) High-performance lithium battery anodes using silicon nanowires. Nat Nanotechnol 3:31–35
81. Yu DP et al (2001) Controlled growth of oriented amorphous silicon nanowires via a solid-liquid-solid (SLS) mechanism. Physica E 9:305–309
82. Kolb FM et al (2004) Analysis of silicon nanowires grown by combining SiO evaporation with the VLS mechanism. J Electrochem Soc 151:G472–G475
83. Chang JB et al (2006) Ultrafast growth of single-crystalline Si nanowires. Mater Lett 60:2125–2128
84. Zhang JG et al (2010) Vapor-induced solid–liquid–solid process for silicon-based nanowire growth. J Power Sources 195:1691–1697
85. Kim H, Han B, Choo J, Cho J (2008) Three-dimensional porous silicon particles for use in high-performance lithium secondary batteries. Angew Chem Int Ed 47:10151–10154
86. Zheng Y, Yang J, Wang JL, NuLi YN (2007) Nano-porous Si/C composites for anode material of lithium-ion batteries. Electrochim Acta 52:5863–5867
87. Xiao J et al (2010) Stabilization of silicon anode for Li-ion batteries. J Electrochem Soc 157: A1047–A1051
88. Ma H et al (2007) Nest-like silicon nanospheres for high-capacity lithium storage. Adv Mater 19:4067–4070
89. Magasinski A et al (2010) High-performance lithium-ion anodes using a hierarchical bottom-up approach. Nat Mat 9:353–358
90. Chen ZH, Christensen L, Dahn JR (2003) Large-volume-change electrodes for Li-ion batteries of amorphous alloy particles held by elastomeric tethers. Electrochem Commun 5:919–923
91. Chen ZH, Christensen L, Dahn JR (2003) Comparison of PVDF and PVDF-TFE-P as binders for electrode materials showing large volume changes in lithium-ion batteries. J Electrochem Soc 150:A1073–A1078
92. Chen ZH, Christensen L, Dahn JR (2004) Mechanical and electrical properties of poly (vinylidene fluoride-tetrafluoroethylene-propylene)/super-S carbon black swelled in liquid solvent as an electrode binder for lithium-ion batteries. J Appl Polym Sci 91:2958–2965
93. Liu WR, Yang MH, Wu HC, Chiao SM, Wu NL (2005) Enhanced cycle life of Si anode for Li-ion batteries by using modified elastomeric binder. Electrochem Solid-State Lett 8: A100–A103

94. Li J, Lewis RB, Dahn JR (2007) Sodium carboxymethyl cellulose – a potential binder for Si negative electrodes for Li-ion batteries. Electrochem Solid-State Lett 10:A17–A20
95. Dimov N, Xia Y, Yoshio M (2007) Practical silicon-based composite anodes for lithium-ion batteries: Fundamental and technological features. J Power Sources 171:886–893
96. Lestrie B, Bahri S, Sandu I, Roue L, Guyomard D (2007) On the binding mechanism of CMC in Si negative electrodes for Li-ion batteries. Electrochem Commun 9:2801–2806
97. Key B et al (2009) Real-time NMR investigations of structural changes in silicon electrodes for lithium-ion batteries. J Am Chem Soc 131:9239–9249
98. Buqa H, Holzapfel M, Krumeich F, Veit C, Novak P (2006) Study of styrene butadiene rubber and sodium methyl cellulose as binder for negative electrodes in lithium-ion batteries. J Power Sources 161:617–622
99. Xu YH, Yin GP, Ma YL, Zuo PJ, Cheng XQ (2010) Simple annealing process for performance improvement of silicon anode based on polyvinylidene fluoride binder. J Power Sources 195:2069–2073
100. Hochgatterer NS et al (2008) Silicon/graphite composite electrodes for high-capacity anodes: Influence of binder chemistry on cycling stability. Electrochem Solid-State Lett 11:A76–A80
101. Guo JC, Wang CS (2010) A polymer scaffold binder structure for high capacity silicon anode of lithium-ion battery. Chem Commun 46:1428–1430
102. Beattie SD, Larcher D, Morcrette M, Simon B, Tarascon JM (2008) Si electrodes for Li-ion batteries – a new way to look at an old problem. J Electrochem Soc 155:A158–A163
103. Zheng Y, Yang J, Tao L, Nuli YN, Wang JL (2007) Study of nano-porous Si/Graphite/C composite anode materials for Li-ion batteries. Chin J Inorg Chem 23:1882–1886
104. Chen LB, Xie XH, Xie JY, Wang K, Yang J (2006) Binder effect on cycling performance of silicon/carbon composite anodes for lithium ion batteries. J Appl Electrochem 36:1099–1104
105. Choi NS, Yew KH, Choi WU, Kim SS (2008) Enhanced electrochemical properties of a Si-based anode using an electrochemically active polyamide imide binder. J Power Sources 177:590–594
106. Liu G (2010) DOE hydrogen program and vehicle technologies program annual merit review and peer evaluation meeting. Department of Energy, Office of Energy Efficiency & Renewable Energy, Washington DC, 2010
107. Zhang JG, Liu J (2010) DOE hydrogen program and vehicle technologies program annual merit review and peer evaluation meeting. Department of Energy, Office of Energy Efficiency & Renewable Energy, Washington DC, 2010
108. Carmer JLG, Morales J, Sanchez L (2008) Nano-Si/cellulose composites as anode materials for lithium-ion batteries. Electrochem Solid-State Lett 11:A101–A104
109. Kulova TL, Skundin AM (2010) Elimination of irreversible capacity of amorphous silicon: direct contact of the silicon and lithium metal. Rus J Electrochem 46:470–475
110. Urbonaite S, Baglien I, Ensling D, Edstrom K (2010) Effect of ethanol-assisted electrode fabrication on the performance of silicon anodes. J Power Sources 195:5370–5373
111. Doh CH et al (2006) Synthesis of silicon-carbon by polyaniline coating and electrochemical properties of the Si-C vertical bar Li cell. Bull Korean Chem Soc 27:1175–1180
112. Choi NS et al (2006) Effect of fluoroethylene carbonate additive on interfacial properties of silicon thin-film electrode. J Power Sources 161:1254–1259
113. Chen LB, Wang K, Xie XH, Xie JY (2007) Effect of vinylene carbonate (VC) as electrolyte additive on electrochemical performance of Si film anode for lithium ion batteries. J Power Sources 174:538–543
114. Han GB, Ryou MH, Cho KY, Lee YM, Park JK (2010) Effect of succinic anhydride as an electrolyte additive on electrochemical characteristics of silicon thin-film electrode. J Power Sources 195:3709–3714
115. Baggetto L et al (2009) On the electrochemistry of an anode stack for all-solid-state 3D-integrated batteries. J Power Sources 189:402–410
116. Arie AA, Chang W, Lee JK (2010) Electrochemical characteristics of semi conductive silicon anode for lithium polymer batteries. J Electroceramics 24:308–312

117. Inose T, Watanabe D, Morimoto H, Tobishima SI (2006) Influence of glyme-based nonaqueous electrolyte solutions on electrochemical properties of Si-based anodes for rechargeable lithium cells. J Power Sources 162:1297–1303
118. Choi NS, Yew KH, Kim H, Kim SS, Choi WU (2007) Surface layer formed on silicon thin-film electrode in lithium bis(oxalato) borate-based electrolyte. J Power Sources 172:404–409
119. Lux SF et al (2010) Li-ion anodes in air-stable and hydrophobic ionic liquid-based electrolyte for safer and greener batteries. Int J Energy Res 34:97–106
120. Cui LF, Yang Y, Hsu CM, Cui Y (2009) Carbon – silicon core – shell nanowires as high capacity electrode for lithium ion batteries. Nano Lett 9:3370–3374
121. Yang Y et al (2010) New nanostructured Li2S/silicon rechargeable battery with high specific energy. Nano Lett 10:1486–1491
122. Arrebola JC et al (2009) Combining 5 V LiNi0.5Mn1.5O4 spinel and Si nanoparticles for advanced Li-ion batteries. Electrochem Commun 11:1061–1064
123. Lee K-L, Jung J-Y, Lee S-W, Moon H-S, Park J-W (2004) Electrochemical characteristics and cycle performance of LiMn2O4/a-Si microbattery. J Power Sources 130:241–246
124. Yin J et al (2006) Micrometer-scale amorphous Si thin-film electrodes fabricated by electron-beam deposition for Li-ion batteries. J Electrochem Soc 153:A472–A477
125. Baranchugov V, Markevich E, Pollak E, Salitra G, Aurbach D (2007) Amorphous silicon thin films as a high capacity anodes for Li-ion batteries in ionic liquid electrolytes. Electrochem Commun 9:796–800
126. Yang H et al (2007) Amorphous Si film anode coupled with $LiCoO_2$ cathode in Li-ion cell. J Power Sources 174:533–537
127. Christensen J (2010) Modeling diffusion-induced stress in Li-Ion cells with porous electrodes. J Electrochem Soc 157:A366–A380
128. Gaines L, a.C., Roy in http://www.transportation.anl.gov/pdfs/TA/149.pdf